Journal of Power Sources 236 (2013) 25–32

Contents lists available at SciVerse ScienceDirect

Journal of Power Sources

journal homepage: www.elsevier.com/locate/jpowsour

Effect of amorphous $FePO_4$ coating on structure and electrochemical performance of $Li_{1.2}Ni_{0.13}Co_{0.13}Mn_{0.54}O_2$ as cathode material for Li-ion batteries

Zhiyuan Wang, Enzuo Liu, Chunnian He, Chunsheng Shi, Jiajun Li, Naiqin Zhao*

School of Materials Science and Engineering, and Tianjin Key Laboratory of Composite and Functional Materials, Tianjin University, Tianjin 300072, PR China

HIGHLIGHTS

- $Li_{1.2}Mn_{0.54}Ni_{0.13}Co_{0.13}O_2$ coated with a uniform layer of $FePO_4$ was synthesized.
- Electrochemical performance was significantly improved by $FePO_4$ coating.
- $FePO_4$ coating layer suppresses the side reactions with the electrolyte.
- $FePO_4$ coating enhances kinetics of $Li_{1.2}Mn_{0.54}Ni_{0.13}Co_{0.13}O_2$ material.

ARTICLE INFO

Article history:
Received 18 November 2012
Received in revised form
29 January 2013
Accepted 8 February 2013
Available online 16 February 2013

Keywords:
Iron phosphate
Coating
Lithium-rich
Cathode
Lithium ion battery

ABSTRACT

Lithium-rich layered cathode $Li_{1.2}Mn_{0.54}Ni_{0.13}Co_{0.13}O_2$ is synthesized by a co-precipitation method followed by high-temperature treatment and surface coated with different amount of amorphous $FePO_4$. The microstructure and electrochemical performance of the as-prepared cathode materials are investigated systematically. It is demonstrated that the $Li_{1.2}Mn_{0.54}Ni_{0.13}Co_{0.13}O_2$ particles are uniformly coated with amorphous $FePO_4$. With proper amount of amorphous $FePO_4$ coating layer, significant improvements in discharge capacity, initial Coulombic efficiency, rate capability, cycle performance, and thermal stability are achieved at room temperature. Specifically, the 3 wt.% $FePO_4$-coated cathode exhibits the highest discharge specific capacities (271.7 mAh g^{-1} at C/20), improved initial Coulombic efficiency (85.1%), and best cyclability (discharge capacity of 202.6 mAh g^{-1} at C/2 after 100 cycles), while the 1 wt.% $FePO_4$-coated cathode displays the best rate capability (194.3 mAh g^{-1} at 1 C rate and 167.9 mAh g^{-1} at 2 C rate). The charge–discharge curves and electrochemical impedance spectra reveal that the improved electrochemical performances are due to the suppression of both the oxygen vacancy elimination at the end of the first charge and side reactions of the cathode with the electrolyte, as well as the decrease in charge transfer polarization by the $FePO_4$ coating layer.

1. Introduction

The increasing demand for high-energy and high-power lithium ion batteries in the development of hybrid electric vehicles (HEVs) and electric vehicles (EVs) has stimulated great research interest in advanced cathode materials for lithium ion batteries (LIBs). Li-rich cathode materials, a series of solid solution between Li_2MnO_3 and $LiMO_2$ (M = Ni, Co, Mn or their combination), have recently attracted particular attention because of their high discharge capacity and low cost compared to the conventional $LiCoO_2$ cathode [1–3]. For example, $xLi_2MnO_3\cdot(1-x)Li[Ni_{1/3}Co_{1/3}Mn_{1/3}]O_2$ (alternately expressed as $Li_{1.2}Mn_{0.54}Ni_{0.13}Co_{0.13}O_2$ when $x = 0.5$) delivers a large capacity over 250 mAh g^{-1} after a first charge at above 4.5 V or higher.

However, there are some issues limiting their adoptability for vehicle applications: (i) large irreversible capacity (C_{irr}) loss during the first cycle; (ii) poor rate capability; (iii) severe cyclic capacity degradation. So for, the large C_{irr} loss is usually attributed to both the extraction of lithium as Li_2O followed by an elimination of oxide ion vacancies from the layered lattice at the end of the first charge and side reactions with the electrolyte at the high operating voltages of up to 4.8 V [4,5]. The poor rate capability could be related to the low electronic conductivity associated with the Li_2MnO_3 and the thick solid-electrolyte interfacial (SEI) layer formed by the aggressive reaction of the cathode surface with the organic electrolytes [5,6].

Surface coatings with stable metal oxides, fluoride or phosphate such as Al_2O_3 [7], AlF_3 [8,9], TiO_2 [10], ZrO_2 [11], RuO_2 [12], ZnO [13],

* Corresponding author. Tel./fax: +86 22 27891371.
E-mail address: nqzhao@tju.edu.cn (N. Zhao).

0378-7753/$ – see front matter © 2013 Elsevier B.V. All rights reserved.
http://dx.doi.org/10.1016/j.jpowsour.2013.02.022

MnO_2 [14], and $AlPO_4$ [15,16] have been proved to be an effective method to protect the cathode from reacting with the electrolyte at high potential to get a longer cycle life. However, some of the coating layers, such as TiO_2 [10] and ZrO_2 [11], are usually electrochemically-inactive materials, so too much coating material on the surface of a cathode material will lead to reduced capacity due to a decrease in active material.

Compared to the above metal oxides, $FePO_4$ as a desirable coating material has been used for enhancing the electrochemical performance of $LiCoO_2$ [17,18], $Li_xNi_{0.9}Co_{0.1}O_2$ [19], $LiMn_2O_4$ [20,21], and $LiMn_{1.5}Ni_{0.5}O_4$ [22] because it is not only chemically-stable but also electrochemically-active. Especially amorphous $FePO_4$ was more reversible compared with crystalline $FePO_4$ due to its porous structure [23–25]. In this paper, the effects of amorphous $FePO_4$ coating on the structure and electrochemical performances of lithium-rich layered cathode material $Li_{1.2}Mn_{0.54}Ni_{0.13}Co_{0.13}O_2$ were investigated and reported for the first time. It is expected that the specific capacity, initial Coulombic efficiency, rate capability, cycle performance and thermal stability would be significantly improved by the amorphous $FePO_4$ coating.

2. Experimental

2.1. Synthesis of $FePO_4$-coated $Li_{1.2}Ni_{0.13}Co_{0.13}Mn_{0.54}O_2$ cathode material

$Li_{1.2}Ni_{0.13}Co_{0.13}Mn_{0.54}O_2$ powder was synthesized by carbonate co-precipitation method followed by high temperature calcination. The spherical $(Mn_{0.66}Ni_{0.17}Co_{0.17})CO_3$ was prepared as follows [26]. An aqueous solution of $NiSO_4$, $CoSO_4$ and $MnSO_4$ (cationic ratio of Ni:Co:Mn = 0.17:0.17:0.66) with a concentration of 2.0 mol L^{-1} was pumped into a continuous stirred reactor. At the same time, 2.0 mol L^{-1} Na_2CO_3 solution with desired amount of $NH_3 \cdot H_2O$ as a chelating agent was also fed into the reactor. The concentration of the solution, pH (8.0), temperature (60 °C), and stirring speed of the mixture in the reactor were carefully controlled. The co-precipitated carbonate precursor $(Mn_{0.66}Ni_{0.17}Co_{0.17})CO_3$ was pre-heated at 550 °C for 5 h in air to decompose the carbonate into an oxide compound. After that, EDTA titration was applied to decide the exact amount of transition metal ions in the pre-heated powder. Then, a 5% excess amount of lithium carbonate (mole ratio, to compensate the portion of lithium evaporation at high temperature) was mixed with the pre-heated powder and calcined at 900 °C for 12 h in air.

In the preparation of the $FePO_4$-coated $Li_{1.2}Ni_{0.13}Co_{0.13}Mn_{0.54}O_2$ cathode material, $Fe(NO_3)_3 \cdot 9H_2O$ (AR) and $(NH_4)_2HPO_4$ were used as starting materials for coating layer. The as-prepared $Li_{1.2}Ni_{0.13}Co_{0.13}Mn_{0.54}O_2$ powder was dispersed into $Fe(NO_3)_3$ aqueous solution and stirring for 30 min to obtain a suspension. Then the $(NH_4)_2HPO_4$ solution was dropped into the suspension with stir. After stirred for 3 h, the mixture was filtered, washed for several times with distilled water, dried at 100 °C for 12 h and subsequently heat-treated in a tube furnace at 400 °C for 5 h in air. By comparison, the pristine $Li_{1.2}Ni_{0.13}Co_{0.13}Mn_{0.54}O_2$ was treated following the same procedures.

2.2. Physical characterization

X-ray diffraction patterns of samples were obtained by an X-ray diffractometer (XRD, Bruker D8 ADVANCE) with a Cu-Kα radiation in a range of 10°–90°. The microstructure of the particles was examined by a field emission scanning electron microscope (FE-SEM, HITACHI S4800) and a high-resolution transmission electron microscope (HRTEM, PHILPS TECNAI G^2 F20). Electron diffraction spectroscopy (EDS) was applied to observe the distribution of elements on the surface of particles together with SEM in large field of view. Information on the surface composition was gathered examined by X-ray photoelectron spectrometer (XPS, Perkin Elmer PHI1600) with a Mg Kα anode (1253.6 eV) as the X-ray source operated in a vacuum of 10^{-7} Torr.

2.3. Electrochemical measurements

Electrode was prepared with a mixture of active material, carbon black, and polyvinylidene fluoride binder dissolved in *N*-methyl-2-pyrrolidone solvent at a weight ratio of 80:10:10. After mixing the slurry thoroughly, it was coated on an aluminum foil current collector, dried at 120 °C overnight in a vacuum oven and cut into a wafer with area of 1.13 cm^2. All types of electrodes comprised ~9 mg of active Li-rich MNC on Al current collector and the thickness of the electrodes is ~44 μm. Then the CR2032 type coin cells were assembled in a Ar-filled glove box using as-prepared $FePO_4$-coated $Li_{1.2}Ni_{0.13}Co_{0.13}Mn_{0.54}O_2$ as cathode, lithium metal as counter electrode and reference electrode, Celgard 2300 polypropylene film as separator and 1 M $LiPF_6$ dissolving in ethylene carbonate (EC)/ethyl methyl carbonate (EMC)/dimethyl carbonate (DEC) (1:1:1 in volume) as electrolyte.

Galvanostatic charge/discharge tests were performed in a voltage range of 2.0–4.8 V with different current densities. The cyclic voltammetry (CV) tests were conducted using a CHI 660D Electrochemical workstation between 2.0 and 4.8 V versus Li^+/Li at a scan rate of 0.2 mV s^{-1} at room temperature. The electrochemical impedance spectroscopy (EIS) of the cells was conducted on an electrochemical workstation (PARSTAT 2273) with an amplitude voltage of 10 mV and frequency range of 10 mHz–100 kHz.

The thermal stability of pristine and 3 wt.% $FePO_4$-coated samples was evaluated by differential scanning calorimeter (NETZSCH DSC 200 F3 Maia). We got the coin cells after the first cycle charged to 4.8 V at 40 mA g^{-1}, and then kept them at that voltage for 1.5 h. The charged cathode samples were achieved from the disassembled cells.

3. Results and discussion

3.1. Structural characterization of pristine and $FePO_4$-coated $Li_{1.2}Ni_{0.13}Co_{0.13}Mn_{0.54}O_2$

The XRD patterns of the pristine powder and the $FePO_4$-coated samples are shown in Fig. 1. All materials exhibit patterns indexed to a layered α-$NaFeO_2$ type structure (space group, $R\bar{3}m$) and some weak peaks in the range of 20–25° corresponding to the superlattice

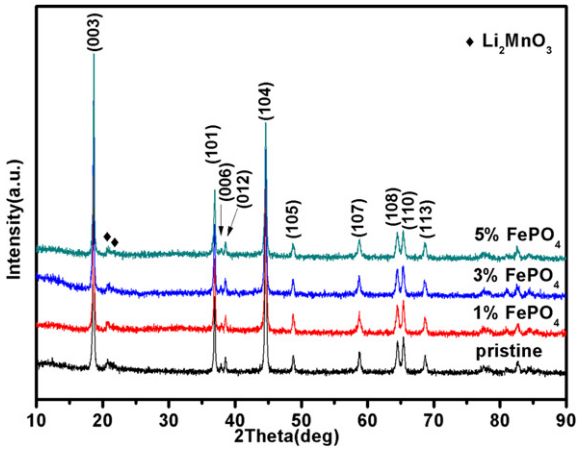

Fig. 1. XRD patterns of pristine and $FePO_4$-coated $Li_{1.2}Ni_{0.13}Co_{0.13}Mn_{0.54}O_2$.

ordered $LiMn_6$ which exists in monoclinic Li_2MnO_3 phase with space group symmetry of C2/m [27,28]. The clear separations between the adjacent peaks of (006)/(102) and (018)/(110) indicate that the samples have a typical well-crystallized layered structure [29,30]. However, there are no distinct diffraction peaks attributed to $FePO_4$ phase in the $FePO_4$-coated $Li[Li_{0.2}Mn_{0.54}Ni_{0.13}Co_{0.13}]O_2$ samples. The absence of the $FePO_4$ peaks suggests two possibilities: the amount of surface coating material is too small to be detected, or the coating layer is poor crystallinity. Since there are still no evident characteristic peaks of $FePO_4$ when the coating amount is increased to 5 wt.%, it can be speculated that the coating layer might be amorphous, which is further confirmed by the following TEM and XPS results. The amorphous $FePO_4$ layer is beneficial for improving the structure stability and electrochemical performance [20–22].

3.2. Morphology of pristine and $FePO_4$-coated $Li_{1.2}Ni_{0.13}Co_{0.13}Mn_{0.54}O_2$

SEM was performed to observe the surface morphology of pristine and $FePO_4$-coated $Li_{1.2}Ni_{0.13}Co_{0.13}Mn_{0.54}O_2$ samples. As shown in Fig. 2, all samples are micro-sized spherical secondary particles with an average diameter of 12 μm, which are aggregated by several primary particles with a diameter in range of 200–300 nm. The tiny primary particles produced by co-precipitation method are very beneficial to Li^+ transfer. Meanwhile, the spherical shape is good for the tap density, which affects the energy density greatly. Furthermore, the $FePO_4$-coated samples are virtually indistinguishable from the pristine sample, except for the slight increase of roughness and diameter due to the thin coating layer. With the amount of $FePO_4$ coating increased from 1 wt.% to 5 wt.%, the coated layer becomes thicker, and the boundaries between the primary particles are more ambiguous. For 3 wt.% $FePO_4$-coated sample, the $FePO_4$ coating layer is very uniform and its thickness is 5–10 nm (Fig. 3). The HRTEM image (Fig. 3(c)) reveals that the formed coating layer is amorphous, which agrees very well with the above XRD results. The $FePO_4$ coating layers are mostly free of defects, which can protect the active materials from directly contacting with the electrolyte and thus can suppress the occurrence of side reactions. In addition, the amorphous $FePO_4$ layer would facilitate the transport of Li ions across the surface compared to a crystalline layer [24,25]. EDS was conducted to check the uniformity of $FePO_4$ coating layer on the surface of 3 wt.% $FePO_4$-coated $Li_{1.2}Ni_{0.13}Co_{0.13}Mn_{0.54}O_2$. As shown in Fig. 4, all the elements especially Fe are distributed homogeneously on the surface of the particles.

3.3. Surface characterization by X-ray photoelectron spectroscopy

In order to investigate the changes of cathode surface property and the chemical state of P in the surface coating layer, XPS was carried out on the samples before and after the $FePO_4$ coating. As shown in Fig. 5, the binding energy of P 2p in the $FePO_4$-coated sample is around 133.01 eV, which is consistent with the value reported for P^{5+} and PO_4 [15,16], while the P 2p peaks in the pristine sample cannot be detected. This observation suggests that the $FePO_4$ coating layer covers the particles of $Li[Li_{0.2}Mn_{0.54}Ni_{0.13}Co_{0.13}]O_2$ effectively.

3.4. Electrochemical characterizations of pristine and $FePO_4$-coated $Li_{1.2}Ni_{0.13}Co_{0.13}Mn_{0.54}O_2$

Fig. 6 shows the first charge–discharge profiles of the pristine and $FePO_4$-coated $Li[Li_{0.2}Mn_{0.54}Ni_{0.13}Co_{0.13}]O_2$ electrodes at

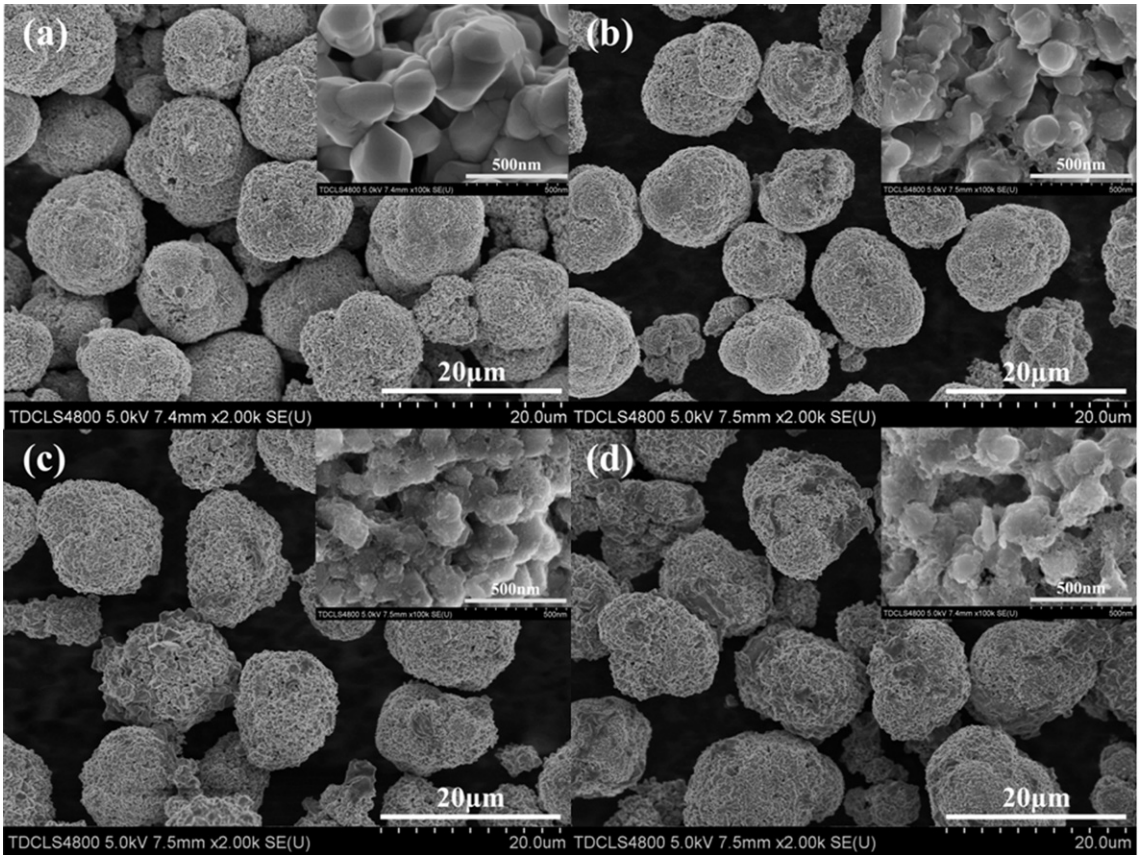

Fig. 2. SEM images of pristine and $FePO_4$-coated $Li_{1.2}Ni_{0.13}Co_{0.13}Mn_{0.54}O_2$: (a) pristine; (b) 1 wt.% $FePO_4$; (c) 3 wt.% $FePO_4$; (d) 5 wt.% $FePO_4$.

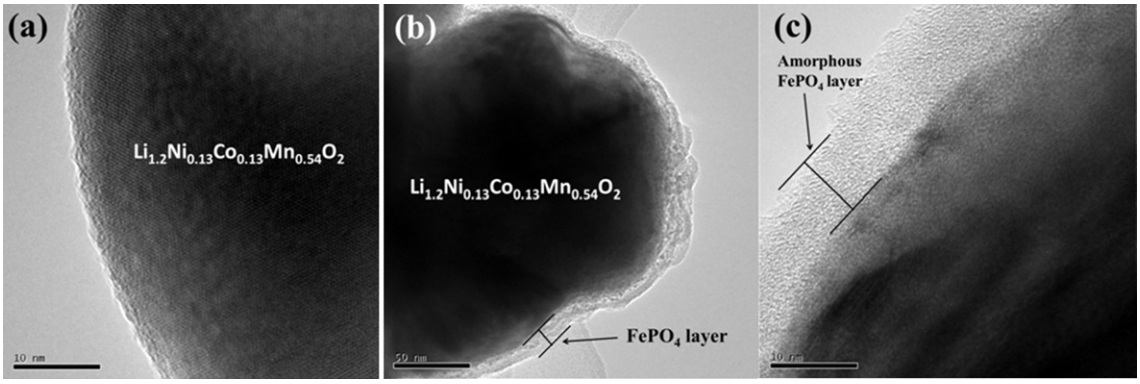

Fig. 3. TEM images of pristine (a) and 3 wt.% $FePO_4$-coated $Li_{1.2}Ni_{0.13}Co_{0.13}Mn_{0.54}O_2$ (b, c).

10 mA g^{-1} (C/20) between 2.0 and 4.8 V. Similar to other Li-enriched cathodes reported [30], all the samples exhibit two plateau regions in the first charge profile that are separated by a dashed vertical line. The initial sloping region A below about 4.5 V corresponds to the lithium extraction first from the layered component ($LiNi_{1/3}Co_{1/3}Mn_{1/3}O_2$), while the plateau region B around 4.5 V is related to simultaneous extraction of lithium and oxygen from the rock salt component Li_2MnO_3 lattice [31,32]. The plateau region B disappears in the subsequent charge profiles, indicating that the oxygen loss during the first charge is an irreversible process. The large irreversible capacity (C_{irr}) loss is due to the elimination of part of the oxide ion vacancies and a corresponding number of lithium ion sites as well as side reactions with the electrolyte at the high operating voltage [4,5]. The first charge/discharge capacity, irreversible capacity and initial Coulombic efficiency values for the pristine and surface-modified samples at C/20 rate are given in Table 1S (Supplementary material). Compared with the pristine sample, the $FePO_4$-coated samples show an increased first discharge capacity and a much reduced C_{irr} value, which can be attributed to the suppression of both the oxide ion vacancy elimination and the side reactions of the electrolyte by the $FePO_4$ coating layer. It is worth noting that the increased first discharge capacity results from the capacity below 3 V regions and the discharge voltage plateau drops correspondingly. We believe that the oxidation and reduction of electrochemically-active amorphous $FePO_4$ can be considered as another reason for the increased discharge capacity.

Cyclic voltammetry was used to investigate the redox reaction occurring during the cycling process (Fig. 7). The cyclic voltammograms of the pristine and coated samples were recorded in the voltage range of 2.0–4.8 V at a scan rate of 0.2 mV s^{-1} for the three cycles. In these CV curves, there are two high anodic peaks. The first anodic peak at approximate 4.0 V in the initial cycle is associated predominantly with Ni oxidation from Ni^{2+} to Ni^{4+}. The second peak at higher potential (4.5–4.8 V) is mainly due to the partial oxidation of Co^{3+} to Co^{4+} and the irreversible electrochemical activation reaction that extraction of Li_2O from the Li_2MnO_3 component to form MnO_2 [33]. The large irreversible capacity is aptly reflected by the second large anodic peak over 4.5 V in the first CV cycle, because the second anodic peak at high potential disappears or reduces to very low after the first cycle. For the CVs of $FePO_4$-coated samples, a low anodic peak and a cathodic peak at approximately 3.0 V become apparent, which can be ascribed to the oxidation and reduction of the iron ions (Fe^{3+}/Fe^{2+}) in amorphous $FePO_4$ (average voltage between reduction and oxidation is almost 3.0 V [24,25]) during the electrochemical reaction. Thus, it is

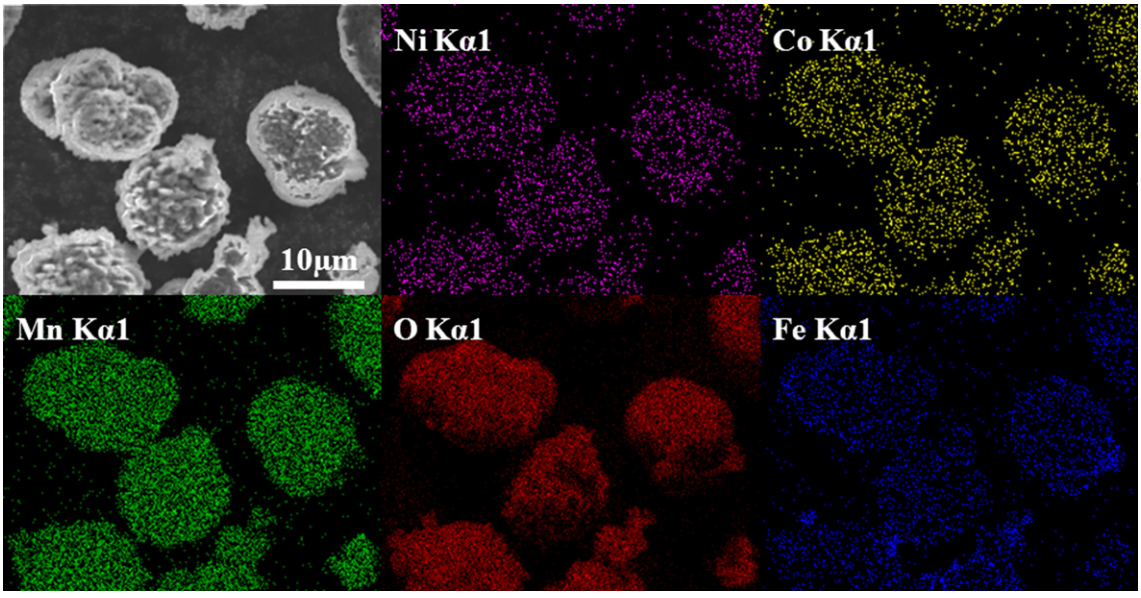

Fig. 4. FE-SEM image and EDS dot-mapping for elements of the 3 wt.% $FePO_4$-coated $Li_{1.2}Ni_{0.13}Co_{0.13}Mn_{0.54}O_2$ powders.

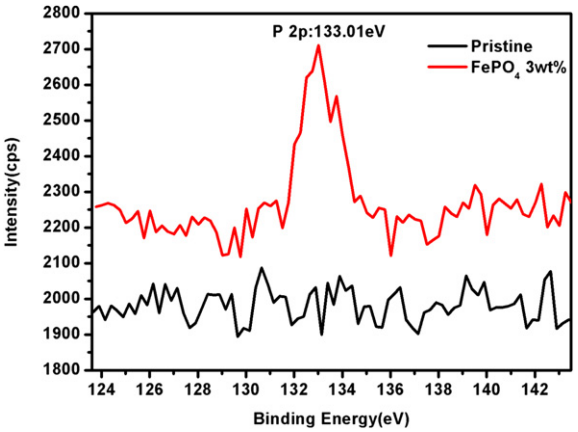

Fig. 5. Comparison of the P 2p XPS spectra of $Li[Li_{0.2}Mn_{0.54}Ni_{0.13}Co_{0.13}]O_2$ before and after coated with 3 wt.% $FePO_4$.

confirmed that $FePO_4$ is electrochemically active with respect to the intercalation and deintercalation of lithium ions for the tested voltages. This result agrees well with the charge and discharge curves.

To study the effect of $FePO_4$ coating on the cycle performance, pristine and $FePO_4$-coated cells were tested by cycling between 2.0 and 4.8 V at C/2 (100 mA g^{-1}) for 100 cycles after ordinal activation at C/20, C/10 and C/5 for one cycle, respectively. As shown in Fig. 8, all the coated samples display more excellent cycle performance and capacity retention than the pristine one. The 3 wt.% coated material has the highest capacity among the four samples. The discharge capacity of the pristine $Li_{1.2}Ni_{0.13}Co_{0.13}Mn_{0.54}O_2$ at C/2 rate changes from 204.3 mAh g^{-1} to 173.5 mAh g^{-1} after 100 cycles with capacity retention of 84.9%. In contrast, the 3 wt.% $FePO_4$-coated $Li_{1.2}Ni_{0.13}Co_{0.13}Mn_{0.54}O_2$ exhibits a higher discharge capacity of 213.7 mAh g^{-1} at C/2 rate and the discharge capacity maintains 203.1 mAh g^{-1} after 100 cycles, with capacity retention of 95.0%. Thus, an appropriate coating amount is critical to the improvement of electrochemical performance. We believe the enhanced cycling performance of $FePO_4$-coated cathode can be attributing to the suppression of side reaction and the decrease in charge transfer resistance, because the amorphous $FePO_4$ coating layer not only plays a role of protective layer to reduce the side reaction between active material and electrolyte but also provides the channels for Li^+ transportation during charging and discharging processes.

To examine rate capability of the pristine and $FePO_4$-coated $Li_{1.2}Ni_{0.13}Co_{0.13}Mn_{0.54}O_2$ electrodes, the cells were first charged and discharged at C/20, C/10 and C/5 for activation, then charged at C/10 and discharged at current rates of C/2, 1 C, 2 C and 5 C (1 C = 200 mA g^{-1}) between 2.0 and 4.8 V vs. Li^+/Li, respectively. The results are shown in Fig. 9 and Fig. 1S (Supplementary material). It is clearly that the $FePO_4$-coated electrode exhibits a superior rate capability than the pristine one. Especially the 3 wt.% $FePO_4$-coated electrode presents the highest capacity at low current density (<C/2) and the 1 wt.% $FePO_4$-coated electrode shows the highest capacity when cycling at high current rates (194.3 mAh g^{-1} at 1 C and 166 mAh g^{-1} at 2 C rate) than the pristine one. When the current rate returns to the low rate current (C/10) after charged and discharged at 5 C, the capacity of sample is retained almost the same value of initial discharge capacity at C/10, which indicates that the cathodes have prefect structural reversibility. The excellent rate capability demonstrates that the amorphous $FePO_4$ coating can effectively enhance the kinetics of $Li_{1.2}Ni_{0.13}Co_{0.13}Mn_{0.54}O_2$, which is further confirmed by the EIS results, as described in the subsequent section.

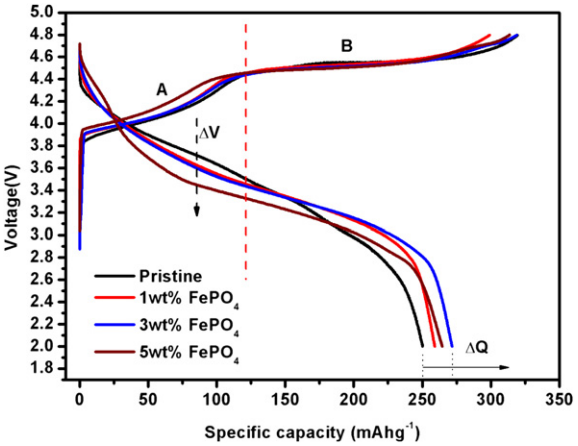

Fig. 6. The initial charge/discharge curves of 0, 1, 3, and 5 wt.% $FePO_4$-coated $Li_{1.2}Ni_{0.13}Co_{0.13}Mn_{0.54}O_2$ cathodes.

3.5. Electrochemical impedance spectra of pristine and $FePO_4$-coated $Li_{1.2}Ni_{0.13}Co_{0.13}Mn_{0.54}O_2$

Electrochemical impedance spectroscopy (EIS) experiments were performed to investigate the impedance variation of the cell prepared with pristine and coated $Li_{1.2}Ni_{0.13}Co_{0.13}Mn_{0.54}O_2$ at the cutoff voltage of 4.3 V at cycle 2 and cycle 42. Nyquist plots of the pristine and the $FePO_4$-coated samples are shown in Fig. 10.

In general, all the spectra consist of two well-defined semicircles and a very short slop line. The semicircle at the higher frequency range reflects the resistance for Li^+ ion migration through the surface films (R_{SEI}), the other one at lower frequency is associated with the charge transfer resistance (R_{ct}), and the slop line at low frequency range reflects Li^+ ion diffusion in the particles of the electrode material [34]. Based on this mechanism, the equivalent circuits for the pristine and surface-modified $Li_{1.2}Ni_{0.13}Co_{0.13}Mn_{0.54}O_2$ samples are given in Fig. 10. As reported, the cell impedance mainly depends on R_{SEI} and R_{ct} [35,36]. Therefore, we focused on the effect of $FePO_4$ coating layer on the two semicircles which are related to the resistance of surface film and charge-transfer. Furthermore, we have calculated the R_{SEI}, R_{ct} and $R_{SEI} + R_{ct}$ values of the pristine and $FePO_4$-coated samples, and the values are presented in Table 1.

As seen from Fig. 10, the diameter of high-frequency semicircle at the 2nd cycle decreases after coating with small amount of $FePO_4$ (1 wt.% and 3 wt.%), and increases slightly when the amount of coated $FePO_4$ reaches 5 wt.%. After 41 cycles, the diameters of high-frequency semicircles for the pristine and the 1 wt.% $FePO_4$-coated samples decrease a little, while for the 3 wt.% and 5 wt.% $FePO_4$-coated samples, it increases. Especially for the 5 wt.% $FePO_4$-coated sample, the diameter of the semicircle at higher frequency increases twice after 41 cycles, which is unfavorable to the rate capability of the cells. The above results indicate that a proper amount of $FePO_4$ coating can effectively suppress the formation of thick SEI layer and decrease the surface film resistance.

The pristine $Li_{1.2}Ni_{0.13}Co_{0.13}Mn_{0.54}O_2$ electrode exhibits a drastic increase in charge-transfer resistance, which can be clearly seen in Fig. 10(a) that the diameter of semicircle at lower frequency significantly increases. As listed in Table 1, R_{ct} value of the pristine sample at the 2nd cycle is small (106.1 Ω cm^2) and rapidly increases to 306 Ω cm^2 after 41 cycles, while the $FePO_4$-coated sample displays much less increase than the pristine sample during cycling, especially for the 1 wt.% and 3 wt.% $FePO_4$-coated samples. However, the R_{ct} for the 5 wt.% $FePO_4$-coated sample at the 2nd cycle increases to 265.7 Ω cm^2 and decreases a little after 41 cycles. The results indicate that a suitable amount of $FePO_4$ coating has an

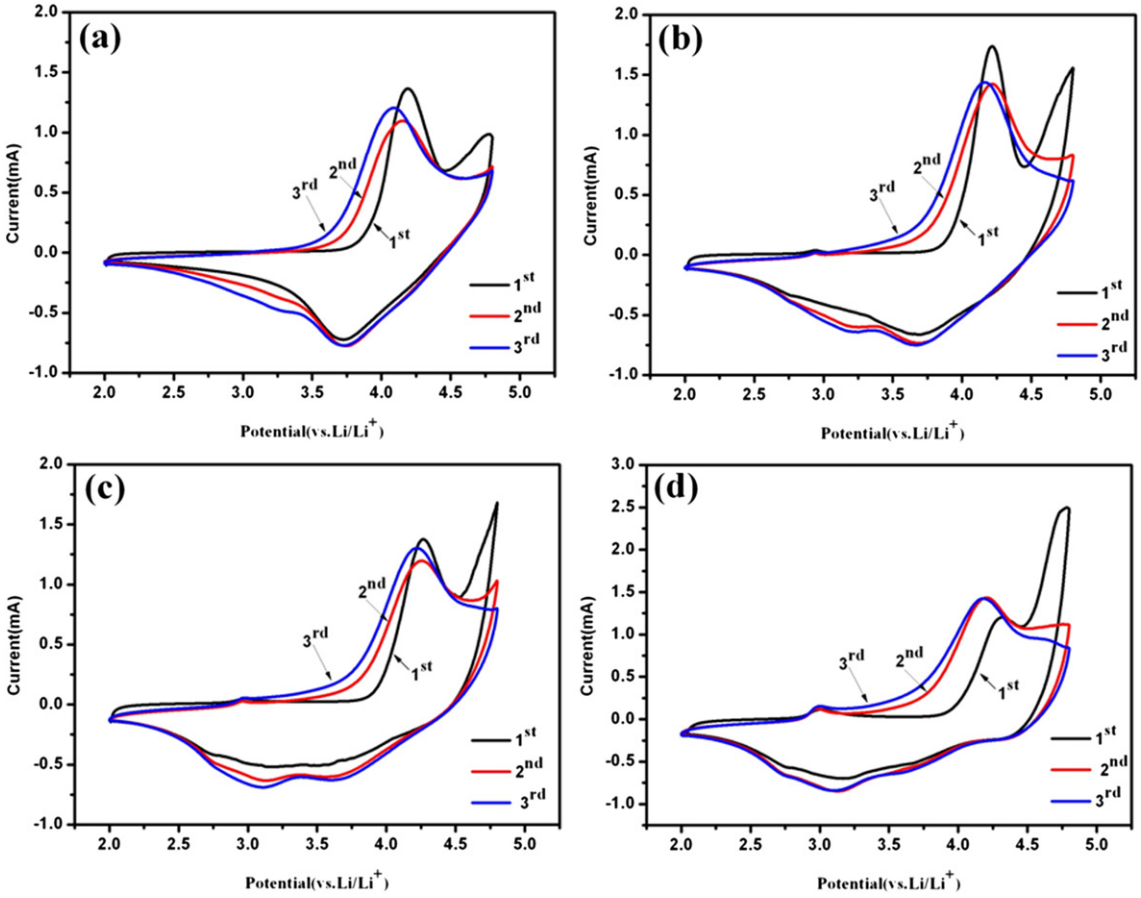

Fig. 7. Cyclic voltammograms for the pristine and $FePO_4$-coated $Li_{1.2}Ni_{0.13}Co_{0.13}Mn_{0.54}O_2$: (a) pristine; (b) 1 wt.% $FePO_4$; (c) 3 wt.% $FePO_4$; (d) 5 wt.% $FePO_4$.

effect on restraining the increase of charge transfer impedance (R_{ct}) and polarization. This can be considered as one of the possible reasons for the enhanced rate capability by $FePO_4$ coating.

3.6. Thermal stability of pristine and $FePO_4$-coated $Li_{1.2}Ni_{0.13}Co_{0.13}Mn_{0.54}O_2$

The thermal stability of cathode materials, especially in the highly delithated state, is one of the most important characteristics in battery safety [37,38]. The thermal stability of the pristine and 3 wt.% $FePO_4$-coated $Li_{1.2}Ni_{0.13}Co_{0.13}Mn_{0.54}O_2$ was measured at 4.8 V using differential scanning calorimetry (DSC), as shown in Fig. 11. The thermal stability of the charged $FePO_4$-coated electrodes is much better than the pristine electrode. The area of the exothermic peak reveals the amount of heat releasing, which generates from the decomposed oxides and the reactions with the electrolyte. The pristine sample shows a large exothermal peak at 279.4 °C with a heat generation of 64.6 J g^{-1}. By contrast, the 3 wt.% $FePO_4$-coated cathode generates only 35.8 J g^{-1} at 285.5 °C (see Fig. 11). It is obvious that the thermal stability is remarkably improved by $FePO_4$ coating modification. The improved thermal stability is ascribed to the amorphous $FePO_4$ coating layer, which protects the highly

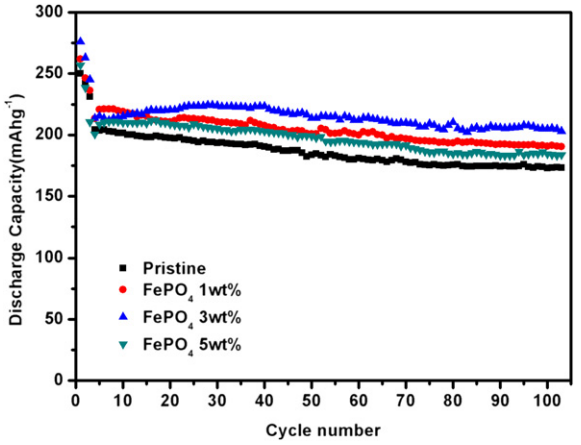

Fig. 8. Cycle performance of Li half-cells for pristine and (1, 3, 5 wt.%) $FePO_4$-coated $Li_{1.2}Ni_{0.13}Co_{0.13}Mn_{0.54}O_2$ cathodes.

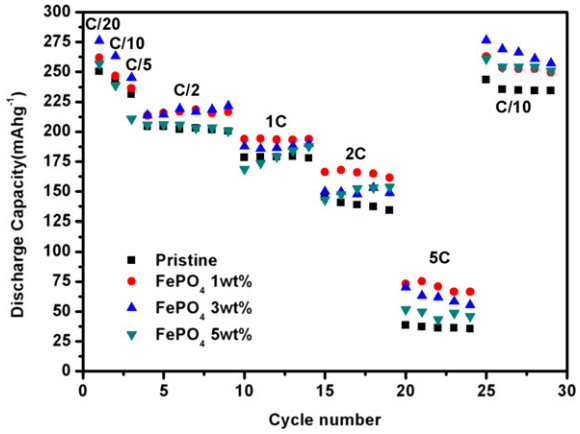

Fig. 9. Rate capability of pristine and (1, 3, 5 wt.%) $FePO_4$-coated $Li_{1.2}Ni_{0.13}Co_{0.13}Mn_{0.54}O_2$ cathodes.

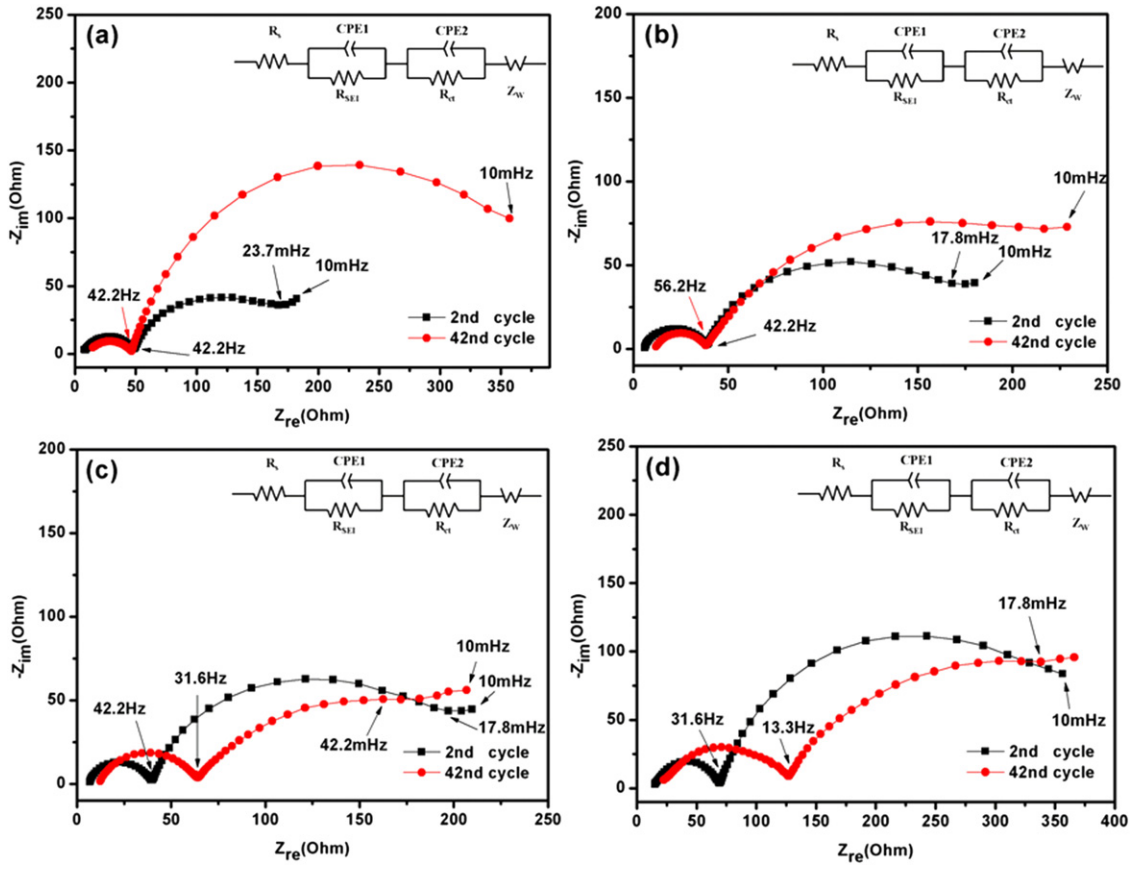

Fig. 10. The Nyquist plots of pristine (a) and 1, 3, 5 wt.% $FePO_4$-coated $Li_{1.2}Ni_{0.13}Co_{0.13}Mn_{0.54}O_2$ (b, c, d).

Table 1
The impedance parameters of equipment circuits.

Samples	R_{SEI} (Ω cm^2)		R_{ct} (Ω cm^2)		$R_{SEI} + R_{ct}$ (Ω cm^2)	
	2nd	42nd	2nd	42nd	2nd	42nd
Pristine	41.4	36.2	106.1	320.0	147.5	356.2
1 wt.% $FePO_4$-coated	30.9	23.6	132.5	172.4	163.4	196.0
3 wt.% $FePO_4$-coated	32.4	51.1	143.6	125.9	176.0	177.0
5 wt.% $FePO_4$-coated	54.5	107.4	265.7	198.1	320.2	305.5

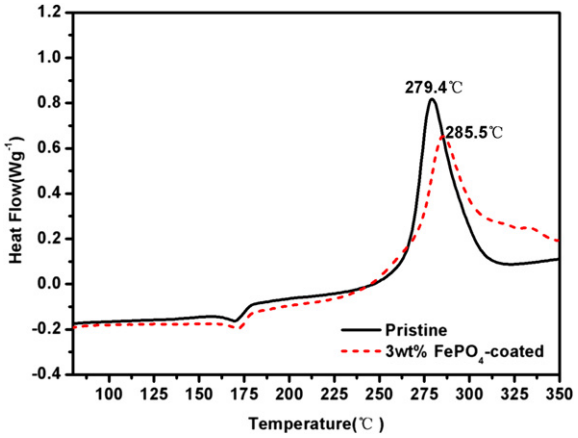

Fig. 11. DSC profiles of pristine and $FePO_4$-coated $Li_{1.2}Ni_{0.13}Co_{0.13}Mn_{0.54}O_2$ after the first cycle and charged to 4.8 V.

oxidized cathode particles from direct contact with the electrolyte solution and thus, reduces the exothermic reaction. We believe that another possible reason for the enhanced thermal stability is that the $FePO_4$ coating layer introduces strong P═O bond on the surface to lower the oxygen activity, which protects the surface of the active material and suppresses the generation of oxygen.

4. Conclusions

The high capacity layered cathode material $Li_{1.2}Mn_{0.54}Ni_{0.13}Co_{0.13}O_2$ coated with different amount of amorphous $FePO_4$ was successfully synthesized. The samples with proper amount of $FePO_4$ exhibit lower irreversible capacity loss C_{irr}, higher discharge capacity, better cycling performance, and rate capability than the pristine material. The improved discharge capacity, initial Coulombic efficiency, and cyclability are due to the high retention of oxide ion vacancies in the layered lattice after the first charge and the suppression of side reaction between active material and electrolyte at high potential. The better rate capability is attributed to a fast charge transfer kinetics arising from the suppression of the undesired SEI layer and the growth of the charge transfer impedance. Therefore, this present amorphous $FePO_4$-coated lithium-rich cathode material $Li_{1.2}Mn_{0.54}Ni_{0.13}Co_{0.13}O_2$ is promising for applications in the fields that require high energy, long calendar life and excellent safety such as electric vehicles.

Acknowledgments

This work was supported by the Key Technologies R & D Program of Tianjin (12ZCZDGX00800), the National Natural Science

Foundation of China (Grants No. 51071107) and the National Basic Research Program of China (Grants No. 2010CB934700).

Appendix A. Supplementary data

Supplementary data related to this article can be found at http://dx.doi.org/10.1016/j.jpowsour.2013.02.022.

References

[1] J.B. Goodenough, Y. Kim, Chemistry of Materials 22 (2010) 587–603.
[2] R. Marom, S.F. Amalraj, N. Leifer, D. Jacob, D. Aurbach, Journal of Materials Chemistry 21 (2011) 9938–9954.
[3] M.M. Thackeray, C. Wolverton, E.D. Isaacs, Energy & Environmental Science 5 (2012) 7854–7863.
[4] M.M. Thackeray, C.S. Johnson, J.T. Vaughey, H.N. Li, S.A. Hackney, Journal of Materials Chemistry 15 (2005) 2257–2267.
[5] M.M. Thackeray, S.-H. Kang, C.S. Johnson, J.T. Vaughey, R. Benedek, S.A. Hackney, Journal of Materials Chemistry 17 (2007) 3112–3125.
[6] Y. Wu, A. Manthiram, Electrochemical and Solid-State Letters 9 (2006) A221–A224.
[7] W.C. West, J. Soler, M.C. Smart, B.V. Ratnakumar, S. Firdosy, V. Ravi, M.S. Anderson, J. Hrbacek, E.S. Lee, A. Manthiram, Journal of The Electrochemical Society 158 (2011) A883–A889.
[8] J.-H. Kim, M.-S. Park, J.-H. Song, D.-J. Byun, Y.-J. Kim, J.-S. Kim, Journal of Alloys and Compounds 517 (2012) 20–25.
[9] Y.-K. Sun, M.-J. Lee, C.S. Yoon, J. Hassoun, K. Amine, B. Scrosati, Advanced Materials 24 (2012) 1192–1196.
[10] J.M. Zheng, J. Li, Z.R. Zhang, X.J. Guo, Y. Yang, Solid State Ionics 179 (2008) 1794–1799.
[11] Y.Y. Huang, J.T. Chen, Jiangfeng Ni, Henghui Zhou, Xinxiang Zhang, Journal of Power Sources 188 (2009) 538–545.
[12] J. Liu, A. Manthiram, Journal of Materials Chemistry 20 (2010) 3961–3967.
[13] G. Singh, R. Thomas, A. Kumar, R.S. Katiyar, A. Manivannan, Journal of The Electrochemical Society 159 (2012) A470–A478.
[14] Y. Zhao, C. Zhao, H. Feng, Z. Sun, D. Xia, Electrochemical and Solid-State Letters 14 (2011) A1–A5.
[15] Q.Y. Wang, J. Liu, A.V. Murugan, A. Manthiram, Journal of Materials Chemistry 19 (2009) 4965–4972.
[16] Y. Wu, A. Vadivel Murugan, A. Manthiram, Journal of The Electrochemical Society 155 (2008) A635–A641.
[17] J. Kim, M. Noh, J. Cho, H. Kim, K.-B. Kim, Journal of The Electrochemical Society 152 (2005) A1142–A1148.
[18] G. Li, Z. Yang, W. Yang, Journal of Power Sources 183 (2008) 741–748.
[19] H. Lee, Y. Kim, Y.-S. Hong, Y. Kim, M.G. Kim, N.-S. Shin, J. Cho, Journal of The Electrochemical Society 153 (2006) A781–A786.
[20] C. Qing, Y. Bai, J. Yang, W. Zhang, Electrochimica Acta 56 (2011) 6612–6618.
[21] Z. Yang, S. Li, S.-A. Xia, Y. Jiang, W.-X. Zhang, Y.-H. Huang, Electrochemical and Solid-State Letters 14 (2011) A109–A119.
[22] D.L. Liu, Y. Bai, S. Zhao, W. Zhang, Journal of Power Sources 219 (2012) 333–338.
[23] W.-j. Cui, H.-j. Liu, C.-x. Wang, Y.-y. Xia, Electrochemistry Communications 10 (2008) 1587–1589.
[24] Y.-S. Hong, K.S. Ryu, Y.J. Park, M.G. Kim, J.M. Lee, S.H. Chang, Journal of Materials Chemistry 12 (2002) 1870–1874.
[25] S. Okada, T. Yamamoto, Y. Okazaki, J.-i. Yamaki, M. Tokunaga, T. Nishida, Journal of Power Sources 146 (2005) 570–574.
[26] D. Wang, I. Belharouak, G.M. Koenig, G. Zhou, K. Amine, Journal of Materials Chemistry 21 (2011) 9290–9295.
[27] K.A. Jarvis, Z. Deng, L.F. Allard, A. Manthiram, P.J. Ferreira, Chemistry of Materials 23 (2011) 3614–3621.
[28] K.A. Jarvis, Z. Deng, L.F. Allard, A. Manthiram, P.J. Ferreira, Journal of Materials Chemistry 22 (2012) 11550–11555.
[29] J. Wang, B. Qiu, H. Cao, Y. Xia, Z. Liu, Journal of Power Sources 218 (2012) 128–133.
[30] H.Z. Zhang, Q.Q. Qiao, G.R. Li, S.H. Ye, X.P. Gao, Journal of Materials Chemistry 22 (2012) 13104–13109.
[31] Y. Wu, A. Manthiram, Journal of Power Sources 183 (2008) 749–754.
[32] N. Yabuuchi, K. Yoshii, S.-T. Myung, I. Nakai, S. Komaba, Journal of the American Chemical Society 133 (2011) 4404–4419.
[33] W. He, J. Qian, Y. Cao, X. Ai, H. Yang, RSC Advances 2 (2012) 3423–3429.
[34] X. Sun, J. Li, C. Shi, Z. Wang, E. Liu, C. He, X. Du, N. Zhao, Journal of Power Sources 220 (2012) 264–268.
[35] C.H. Chen, J. Liu, K. Amine, Journal of Power Sources 96 (2001) 321–328.
[36] J. Liu, A. Manthiram, Chemistry of Materials 21 (2009) 1695–1707.
[37] Y.-K. Sun, Z. Chen, H.-J. Noh, et al., Nature Materials (2012). http://dx.doi.org/10.1038/nmat3435.
[38] W. Chang, J.-W. Choi, J.-Ch. Im, et al., Journal of Power Sources 195 (2010) 320–326.